Angewandte Zuschriften

Water

DOI: 10.1002/ange.201403839

Size-Dependent Water Structures in Carbon Nanotubes**

*Tomonori Ohba**

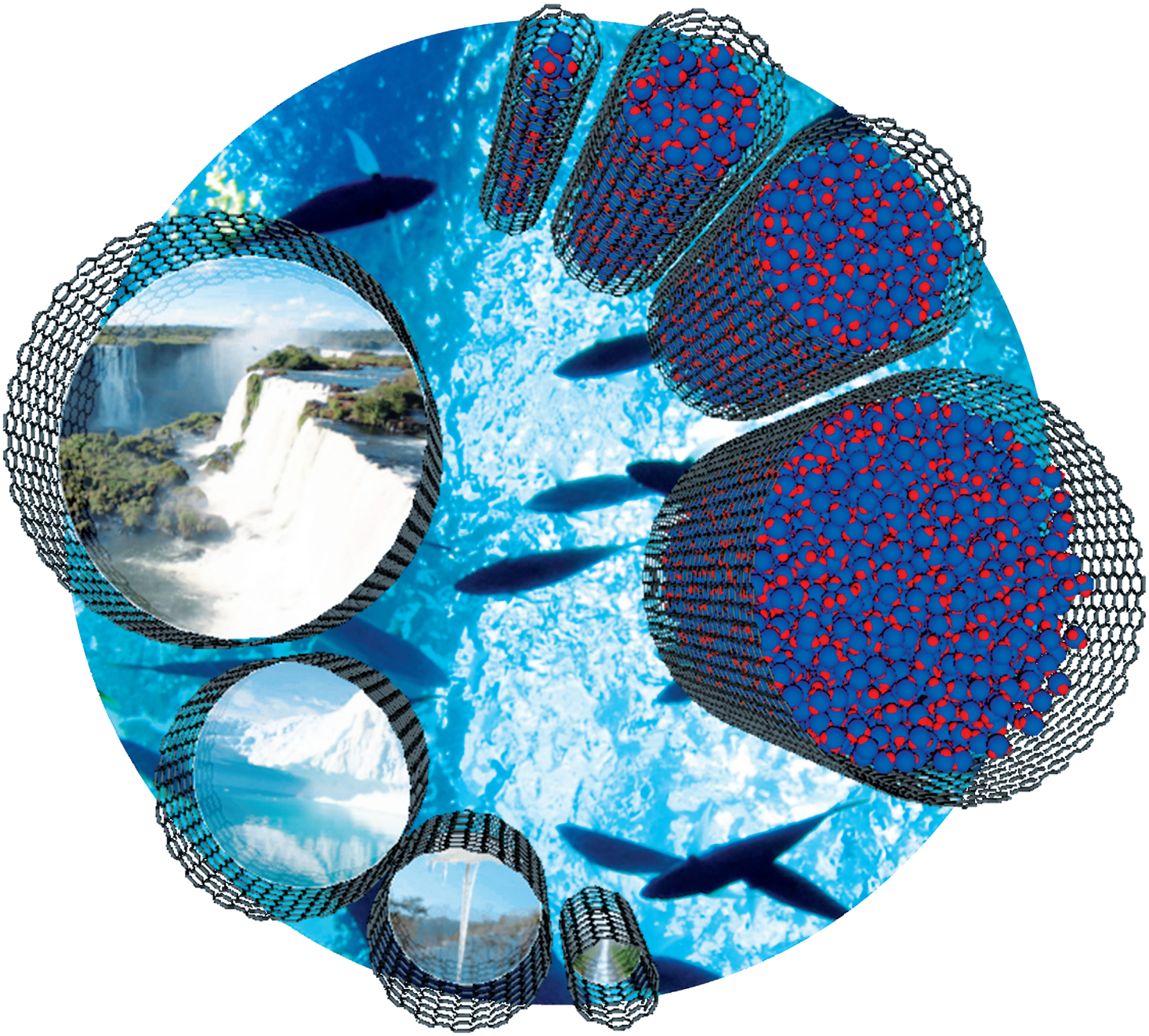

Angewandte Chemie

Abstract: *Water surrounded by hydrophobic interfaces affects a variety of chemical reactions and biological activities. Carbon nanotubes (CNTs) can be used to investigate the behavior of water at hydrophobic interfaces. Here, we determined the fundamental unit of water by evaluating the ice-like cluster formation of water in the limited hydrophobic nanospaces of CNTs, using X-ray diffraction and molecular simulation analysis. The water in CNTs with a diameter of 1 nm had fewer hydrogen bonds than bulk water under ambient conditions. In CNTs with diameters of 2 and 3 nm, water formed nanoclusters even under ambient conditions, because of prolific hydrogen bonding; predominant ice-like cluster formation was induced in the 2–3 nm nanospaces. The results confirming the cluster formation in the CNTs also demonstrated that the critical cluster size was 0.8–3.4 nm. The fundamental cluster size was 0.8 nm; these results indicated that 0.8 nm clusters are the fundamental units of water assemblies.*

The strong hydrogen bonds in water greatly affect water structures.[1] Water at hydrophobic interfaces also influences the biological activity in water channels, and a variety of chemical reactions. The complex behavior and unique structural formations of water at hydrophobic interfaces are attributed to hydrogen bonding, despite the fact that the water in such environments shows hydrogen bonding that is weak compared with that of bulk water; in contrast, strong hydrogen bonding is observed at hydrophilic interfaces.[2] As examples of such complex behavior, interfacial water showed different relaxation pathways at interfaces,[2a,b] non-hydrogen-bonded OH groups of water that differed from those found for bulk water were observed at molecular hydrophobic interfaces,[2c,d] unusual stretching of water was noted in carbon nanotubes (CNTs),[2e] and ring-like ice formation in CNTs at room temperature and under extremely high pressures was predicted using molecular dynamics simulations.[2f] The water in hydrophobic carbon nanospaces is changed from hydrophobic to hydrophilic as water is introduced and the temperature decreases.[3] Such hydrophobic carbon nanospaces also induce unique flow properties in water. Holt and co-workers first demonstrated the rapid flow of water through CNT membranes.[4] Furthermore, water flows faster through narrower CNTs.[5] The sequential flow of water through CNTs occurs via the structural transformation of water from clusters to monolayers during loading and release processes.[6] Molecular dynamics simulations revealed the mechanism of the water flow through CNTs.[7] The hydrogen bonds of water in a CNT are highly restricted, but water can freely rotate,[7a] and the hydrogen bonds promote the rapid flow of water through a CNT.[7b] Water cluster-mediated diffusion in CNTs has also been predicted.[7c] The promotion of rapid water flow through CNTs was also observed experimentally, when the relationship between the water flow rate and hydrogen bonding was examined.[5b] In contrast, the direct observation of water confined in CNTs using transmission electron microscopy revealed slow water flow, and complex meniscus shapes.[8] Overall, the mechanism of water flow in CNTs remains unclear.

The complex properties of water in CNTs intrigue scientists, but no conclusion has yet been reached (backed by experimental evidence) regarding the mechanism responsible for these properties. The structural evaluation of water in CNTs is therefore important for the understanding of the fundamental properties of water under such conditions. Ice phases were observed in CNTs with diameters of 1–2 nm in canonical ensemble molecular dynamics simulations,[9] not only at high pressure,[2f] but also at ambient pressure. Ice-like cluster formation was also observed experimentally in CNTs with a diameter of 2 nm under ambient conditions, using X-ray structure analysis.[10] Ice peaks were observed in the X-ray diffraction (XRD) patterns of water in CNTs at low temperature, suggesting the formation of pentagonal and octagonal ice nanotubes.[11] Such ice formation was attributed to strong hydrogen bonding. However, hydrogen bond formation is restricted in the hydrophobic nanospaces of CNTs.[2c,d,5b,7b] The CNT diameter strongly affects the hydrogen bonding, because a CNT provides a highly restricted one-dimensional nanospace. On the other hand, no hydrogen bonding of water was observed in the zero-dimensional nanospaces of fullerene.[12] Thus, CNTs are ideal limited nanospaces to evaluate the fundamental unit of water. It is desirable to examine the dependence of the hydrogen bonding and the ice-like cluster formation on the CNT diameter, to better understand the properties of water in CNTs. In this study, we determined the structure of water in CNTs of various diameters using XRD analysis and hybrid reverse Monte Carlo (HRMC) simulations.

The nanospace structures of the CNTs were assessed using transmission electron microscopy (as shown in Figure 1), Raman spectroscopy, and N_2 adsorption isotherms (as shown in Figure S1). The average diameters of the internal nanospaces of CNTs (evaluated from these measurements) were approximately 1, 2, 3, and 5 nm, so these CNTs were named as 1 nm, 2 nm, 3 nm, and 5 nm CNTs, respectively. Water vapor could be adsorbed both in the internal and external nanospaces of the CNTs. However, a geometrical assessment (Figure S2) showed that the amount of water vapor adsorbed in the internal nanospaces was significantly larger than the amount of water vapor adsorbed in the external nanospaces.

Figure 2a and b shows XRD patterns for water-adsorbed CNTs and bulk water, and electron radial distribution functions calculated from the differential XRD patterns (Figure S3). The XRD patterns in Figure 2a included water-water, water-CNTs, and CNT-CNT correlations. The scattering between the CNTs could be removed by subtracting the

[*] Prof. Dr. T. Ohba
Graduate School of Science, Chiba University
1-33 Yayoi, Inage, Chiba 263-8522 (Japan)
E-mail: ohba@pchem2s.chiba-u.ac.jp

[**] We thank Dr. K. Hata of the AIST for supplying carbon nanotubes, and Dr. J. Kim, Dr. N. Tsuji, and Dr. S. Kohara for their help in recording the XRD data at Spring-8. This research was supported by a JSPS KAKENHI (grant number 26706001) and Research Fellowships from the Futaba Electronics Memorial Foundation, Foundation for the JGC-S Scholarship Foundation, Promotion of Ion Engineering, and Murata Science Foundation.

Supporting information for this article is available on the WWW under http://dx.doi.org/10.1002/anie.201403839.

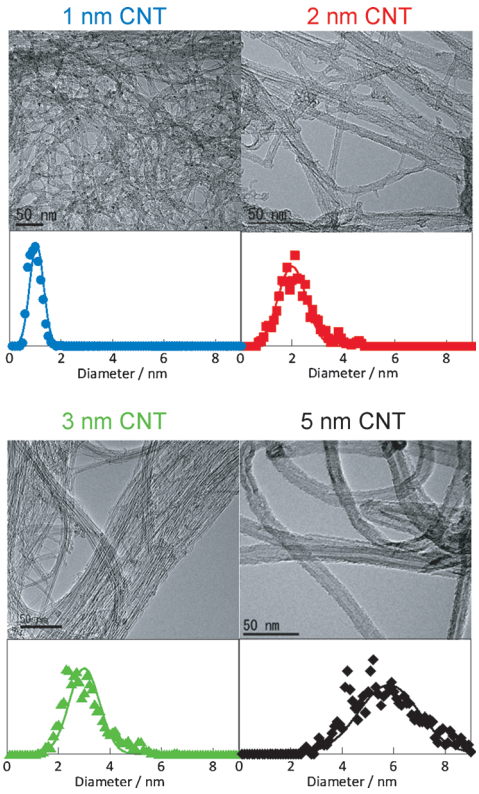

Figure 1. CNT diameter distributions obtained from approximately 1000 CNTs observed in transmission electron microscopy images. The average tube diameters were 1.0, 2.1, 2.9, and 5.7 nm for the 1, 2, 3, and 5 nm CNTs, respectively. All scale bars are 50 nm.

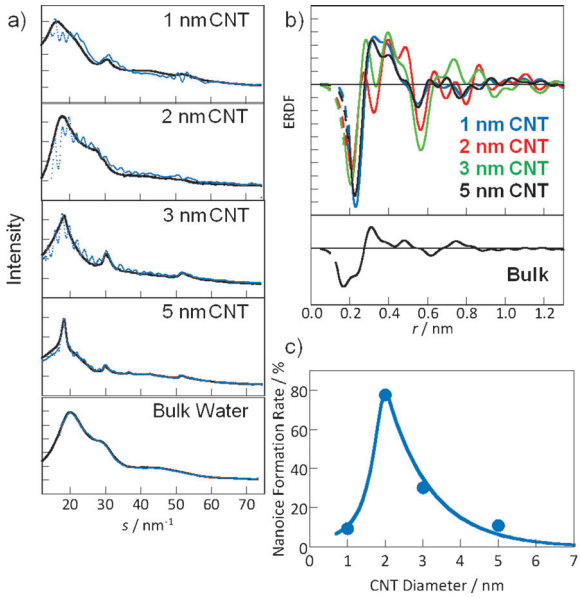

Figure 2. Ice formation in water confined in hydrophobic CNTs. a) XRD patterns for CNTs containing confined water, and bulk water, and corresponding HRMC-simulated XRD patterns. s is defined as $4\pi\sin(\theta)/\lambda$, where λ is the X-ray wavelength. The black and blue curves represent the XRD patterns and the HRMC-simulated XRD patterns, respectively. b) Electron radial distribution functions of water confined in CNTs, obtained from Fourier transforms of the differential XRD patterns for dry CNTs, and those containing confined water. The electron radial distribution functions for bulk water are also shown, for comparison. c) Dependence of the nanosize ice formation on the CNT diameter, calculated from the deconvolution of the first XRD peak with two components of the XRD peaks for simulated 1 nm ice and bulk water.

difference between the XRD patterns for the CNTs and the patterns for the CNTs containing adsorbed water, as shown in Figure S2. As water-CNT scatterings in the differential XRD patterns were experimentally remained, the differential XRD patterns and the electron radial distributions included both water-water and water-CNT scattering. Only the water-water scattering could be extracted using the HRMC simulations, as described later. The electron radial distribution of the bulk water corresponded well with reported values; the first, second, and third major peaks appeared at 0.31, 0.48, and 0.75 nm, respectively.[1b,13] The electron radial distributions of the water in the CNTs were significantly different from that of the bulk water. For water in the 1 nm CNT, the first peak was found at 0.31 nm, corresponding to the peak position of bulk water, and further peak also appeared at 0.38 nm. However, at distances longer than 0.6 nm, the correlations between the water molecules shown in the electron radial distributions of the bulk water and the water confined in the 1 nm CNTs were weak. These tendencies were very similar to the electron radial distribution in the 5 nm CNTs. Conversely, the electron radial distributions in the 2 nm and 3 nm CNTs showed patterns that were considerably different from those of the other samples. The peaks appeared at longer distances, and the peak positions were shifted; for instance, the first peak shifted from 0.31 to 0.27 nm. Peaks were observed at 0.27, 0.38, 0.48, 0.63, 0.73, and 0.86 nm. The ideal intermolecular distances in hexagonal ice are 0.28, 0.39, 0.46, 0.54, and 0.65 nm.[14] Therefore, ice structures might have formed in the 2 nm and 3 nm CNTs at ambient temperature.

The XRD patterns around the first peaks were deconvoluted using the XRD patterns for nanosized ice and liquid water, to evaluate whether the water in the CNTs formed ice- or liquid-like structures (Figure S3). Figure 2c shows the proportion of nanosized ice formations in the CNTs, which was defined as the deconvoluted peak intensity of the first peak for nanosized ice to the sum of the intensities of the peaks for nanosized ice and liquid water. Ice-like structures were observed in the CNTs even at ambient temperature; the proportions of ice in the 1 nm, 2 nm, 3 nm, and 5 nm CNTs were approximately 10%, 80%, 30%, and 10%, respectively. Thus, the nanospaces of the CNTs induced the water contained in them to form ice-like structures, even at ambient temperature, particularly in the 2 nm CNTs. In contrast, liquid-like structures were observed in the extremely narrow nanospaces of the 1 nm CNTs, showing features that were rather different compared with those displayed in narrow hydrophilic nanospaces.[2g]

HRMC-simulated XRD patterns for water in the different CNTs are shown in Figure 2a alongside the experimental XRD patterns. A comparison of these patterns indicated that good agreement was shown between the simulated and experimental XRD patterns. Slight differences were observed, because of the assumption of an idealized CNT

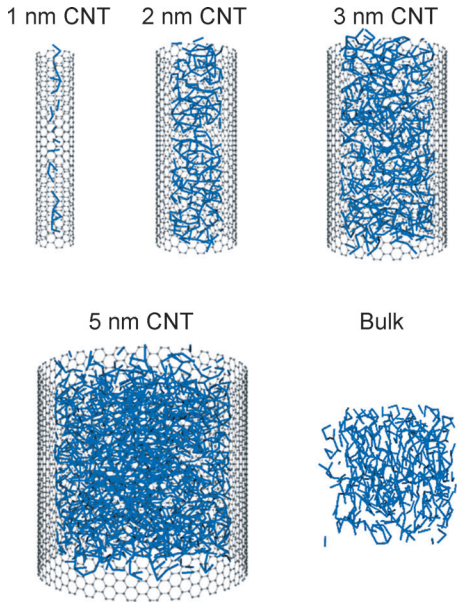

Figure 3. Snapshots of the hydrogen bonding of water in CNTs and in bulk water, in HRMC simulations. The blue lines represent hydrogen bonds between water. Carbon atoms and C–C bonds are depicted as black spheres and lines, respectively.

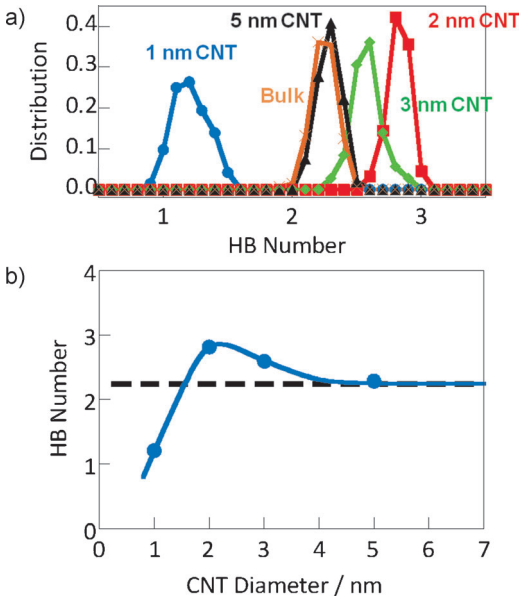

Figure 4. Hydrogen bonding of water in CNTs. a) Distributions of the hydrogen bond numbers of water confined in the CNTs and in bulk water, estimated from the snapshots of hydrogen bonds shown in Figure 3. b) Dependence of the mean hydrogen-bond number on the CNT diameter. The dashed line represents the mean hydrogen bond number in bulk water.

structure. Figure 3 shows snapshots of the hydrogen bonds of the water in the CNTs, as evaluated from the HRMC simulations (Figure S4). Here, a hydrogen bond was assumed to form when the O···H distance was less than 0.25 nm and the angle of the OH···lone pair was larger than 140°; these values were similar to the values used in previous studies.[15] The hydrogen bonds formed predominantly along the CNT axis in the 1 nm CNTs. In contrast, a three-dimensional network of hydrogen bonds formed in the other CNTs and in the bulk water, although it was restricted at the interface between the water and the CNT. The water could therefore form enough hydrogen bonds to produce a three-dimensional network in the hydrophobic nanospaces of the CNTs, except in the case of the CNTs with a diameter of 1 nm. The distributions of the numbers of hydrogen bonds presented in Figure 4a were calculated from the hydrogen bond connections shown in Figure 3. A mean hydrogen bond number was also calculated from each distribution of hydrogen bond number, as shown in Figure 4b. The number of hydrogen bonds in the bulk water was 2.2, a number that was somewhat smaller than the numbers obtained using other techniques.[15a,16] Here, only the strong hydrogen bonds were assessed. The number of hydrogen bonds in the water in the 5 nm CNTs was equivalent to that in the bulk water, while the number of hydrogen bonds in the 1 nm CNT, 1.2, was much lower than the numbers determined for the other CNTs. The number of hydrogen bonds in the water condensed in the 1 nm CNT was intermediate between the number of hydrogen bonds in liquid and vapor. Thus, the water formed a supercritical gas-like structure in the 1 nm CNT. In contrast, the water in the 2 nm and 3 nm CNTs contained considerably higher numbers of hydrogen bonds compared with the water in the other CNTs, although the structures were less crystalline than the ice structures. The prolific formation of hydrogen bonds in the 2 nm and 3 nm CNTs therefore induced nanocluster formation. Ice-like crystalline structures were observed in the hydrophilic nanospaces of nanocontainers, and thus each water molecule formed approximately four hydrogen bonds.[17] The hydrogen bonding in the hydrophobic nanospaces of CNTs was significantly restricted compared with that occurring in hydrophilic nanospaces.

The mean hydrogen bond number is shown as a function of CNT diameter in Figure 4b; these results showed that the diameters of the CNTs containing water with a higher hydrogen bond number than that of bulk water lay in the range from 1.5 to 4.0 nm. This range of CNT diameters approximately corresponded to the diameters of the CNTs showing substantial nanocluster formation (with a proportion of nanocluster formation higher than 20%), as shown in Figure 2c. The effective nanospace diameters for water vapor adsorption for the CNTs with diameters of 1.5–4.0 nm were 0.8–3.4 nm, according to the relationship between the effective nanospace diameter and the actual CNT diameter (Supplementary Figure S5). Thus, effective nanospaces with diameters of 0.8–3.4 nm induced water to form nanoclusters under ambient conditions. In other words, the size of the water clusters was 0.8–3.4 nm. Stable water cluster structures show a ring-like structure for numbers smaller than five, and a cage-like structure for numbers larger than six.[18] The size of the water clusters, 0.8–3.4 nm, corresponded to clusters with a size of approximately 8–600 molecules, according to the size evaluations performed using the cage model described in the literature, and the density of liquid water.[18c]

The water confined in the CNTs with average diameters of 2 and 3 nm formed clusters preferentially, even under ambient conditions, whereas the water tended to be supercritical gas-

like and liquid-like in the CNTs with average diameters of 1 and 5 nm, respectively. The cluster structures of the water in the CNTs with average diameters of 2 and 3 nm were caused by significant levels of hydrogen bond formation. The dependence of the nanocluster formation and the hydrogen bond number on the CNT diameter suggested that the effective nanospace diameters needed for the nanocluster formation of water were 0.8–3.4 nm. Thus, the structural transformations from vapor to supercritical gas-like water, liquid-like water, and water clusters were imposed by the size of the CNT nanospaces and the fundamental cluster size is 0.8 nm.

Received: March 31, 2014
Published online: June 4, 2014

Keywords: hydrogen bonds · nanostructures · nanotubes · water chemistry · X-ray diffraction

[1] a) I. Brovchenko, A. Geiger, A. Oleinikova, *J. Chem. Phys.* **2005**, *123*, 044515; b) A. K. Soper, M. A. Ricci, *Phys. Rev. Lett.* **2000**, *84*, 2881 – 2884; c) C. Huang, K. T. Wikfeldt, T. Tokushima, D. Nordlund, Y. Harada, U. Bergmann, M. Niebuhr, T. M. Weiss, Y. Horikawa, M. Leetmaa, M. P. Ljungberg, O. Takahashi, A. Lenz, L. Ojamae, A. P. Lyubartsev, S. Shin, L. G. Pettersson, A. Nilsson, *Proc. Natl. Acad. Sci. USA* **2009**, *106*, 15214 – 15218; d) F. N. Keutsch, R. J. Saykally, *Proc. Natl. Acad. Sci. USA* **2001**, *98*, 10533 – 10540.

[2] a) C. S. Hsieh, R. Kramer Campen, M. Okuno, E. H. G. Backus, Y. Nagata, M. Bonn, *Proc. Natl. Acad. Sci. USA* **2013**, *110*, 18780 – 18785; b) C. S. Tian, Y. R. Shen, *J. Am. Chem. Soc.* **2009**, *131*, 2790 – 2791; c) L. F. Scatena, M. G. Brown, G. L. Richmond, *Science* **2001**, *292*, 908 – 912; d) J. G. Davis, B. M. Rankin, K. P. Gierszal, D. Ben-Amotz, *Nat. Chem.* **2013**, *5*, 796 – 802; e) O. Byl, J. C. Liu, Y. Wang, W. L. Yim, J. K. Johnson, J. T. Yates, Jr., *J. Am. Chem. Soc.* **2006**, *128*, 12090 – 12097; f) K. Koga, G. Gao, H. Tanaka, X. C. Zeng, *Nature* **2001**, *412*, 802 – 805; g) R. Costard, I. A. Heisler, T. Elsaesser, *J. Phys. Chem. Lett.* **2014**, *5*, 506 – 511.

[3] a) H. J. Wang, X. K. Xi, A. Kleinhammes, Y. Wu, *Science* **2008**, *322*, 80 – 83; b) T. Ohba, H. Kanoh, K. Kaneko, *J. Am. Chem. Soc.* **2004**, *126*, 1560 – 1562.

[4] J. K. Holt, H. G. Park, Y. Wang, M. Stadermann, A. B. Artyukhin, C. P. Grigoropoulos, A. Noy, O. Bakajin, *Science* **2006**, *312*, 1034 – 1037.

[5] a) X. Qin, Q. Yuan, Y. Zhao, S. Xie, Z. Liu, *Nano Lett.* **2011**, *11*, 2173 – 2177; b) T. Ohba, K. Kaneko, M. Endo, K. Hata, H. Kanoh, *Langmuir* **2013**, *29*, 1077 – 1082; c) A. Kalra, S. Garde, G. Hummer, *Proc. Natl. Acad. Sci. USA* **2003**, *100*, 10175 – 10180.

[6] T. Ohba, S. Taira, K. Hata, H. Kanoh, *J. Phys. Chem. Lett.* **2013**, *4*, 1211 – 1215.

[7] a) G. Hummer, J. C. Rasaiah, J. P. Noworyta, *Nature* **2001**, *414*, 188 – 190; b) S. Joseph, N. R. Aluru, *Nano Lett.* **2008**, *8*, 452 – 458; c) A. Striolo, *Nano Lett.* **2006**, *6*, 633 – 639; d) A. Berezhkovskii, G. Hummer, *Phys. Rev. Lett.* **2002**, *89*, 064503; e) J. A. Thomas, A. J. McGaughey, *Nano Lett.* **2008**, *8*, 2788 – 2793.

[8] a) N. Naguib, H. Ye, Y. Gogotsi, A. G. Yazicioglu, C. M. Megaridis, M. Yoshimura, *Nano Lett.* **2004**, *4*, 2237 – 2243; b) M. P. Rossi, H. Ye, Y. Gogotsi, S. Babu, P. Ndungu, J.-C. Bradley, *Nano Lett.* **2004**, *4*, 989 – 993.

[9] D. Takaiwa, I. Hatano, K. Koga, H. Tanaka, *Proc. Natl. Acad. Sci. USA* **2008**, *105*, 39 – 43.

[10] T. Ohba, S. Taira, K. Hata, K. Kaneko, H. Kanoh, *RSC Adv.* **2012**, *2*, 3634 – 3637.

[11] Y. Maniwa, H. Kataura, M. Abe, A. Udaka, S. Suzuki, Y. Achiba, H. Kira, K. Matsuda, H. Kadowaki, Y. Okabe, *Chem. Phys. Lett.* **2005**, *401*, 534 – 538.

[12] K. Kurotobi, Y. Murata, *Science* **2011**, *333*, 613 – 616.

[13] a) F. Paesani, G. A. Voth, *J. Phys. Chem. B* **2009**, *113*, 5702 – 5719; b) T. Ohba, K. Hata, H. Kanoh, *J. Am. Chem. Soc.* **2012**, *134*, 17850 – 17853.

[14] A. Leadbetter, R. Ward, J. Clark, P. Tucker, T. Matsuo, H. Suga, *J. Chem. Phys.* **1985**, *82*, 424.

[15] a) T. Werder, J. H. Walther, R. Jaffe, T. Halicioglu, P. Koumoutsakos, *J. Phys. Chem. B* **2003**, *107*, 1345 – 1352; b) J. Martí, M. C. Gordillo, *J. Chem. Phys.* **2003**, *119*, 12540.

[16] R. J. Mashl, S. Joseph, N. R. Aluru, E. Jakobsson, *Nano Lett.* **2003**, *3*, 589 – 592.

[17] a) A. Müller, E. Krickemeyer, H. Bögge, M. Schmidtmann, B. Botar, M. O. Talismanova, *Angew. Chem.* **2003**, *115*, 2131 – 2136; *Angew. Chem. Int. Ed.* **2003**, *42*, 2085 – 2090; b) T. Mitra, P. Miro, A. R. Tomsa, A. Merca, H. Bogge, J. B. Avalos, J. M. Poblet, C. Bo, A. Muller, *Chem. Eur. J.* **2009**, *15*, 1844 – 1852.

[18] a) S. S. Xantheas, *J. Chem. Phys.* **1995**, *102*, 4505; b) B. Q. Ma, H. L. Sun, S. Gao, *Chem. Commun.* **2004**, 2220 – 2221; c) S. Maheshwary, N. Patel, N. Sathyamurthy, A. D. Kulkarni, S. R. Gadre, *J. Phys. Chem. A* **2001**, *105*, 10525 – 10537; d) A. Müller, M. Henry, *C. R. Chim.* **2003**, *6*, 1201 – 1208.

